Istraživanja i projektovanja za privredu
ISSN 1451-4117
DOI:10.5937/jaes0-43529
www.engineeringscience.rs

iipp publishing

Journal of Applied Engineering Science
Vol. 21, No. 3, 2023
Original Scientific Paper
Paper number: 21(2023)3, 1128, 859-871

DYNAMIC RESPONSE OF HIGH-POWER ULTRASONIC SYSTEM BASED ON FINITE ELEMENT MODELING OF PIEZOELECTRIC

Viet Dung Luong[1]*, Pham Tuong Minh Duong[1], Thi Bich Ngoc Nguyen[1], Nhu Khoa Ngo[1], Thi Hoa Nguyen[1], Van Du Nguyen[1]

[1] Faculty of Mechanical Engineering, Thai Nguyen University of Technology, 3/2 street, Tich luong ward, Thai Nguyen City 251750, Vietnam

** luongvietdung@tnut.edu.vn*

In this study, a new finite element model for ultrasonic welding equipment is proposed. This help to solve remaining issues such as element type selection for the numerical model, mesh size, and how to determine the parameters of piezoelectric materials. The obtained results clearly show the influence of element type and mesh size on resonance frequency and amplitude. Specifically, with a mesh size of 2 mm, it was concluded to be suitable for the model. For the C3D8 element (C3D8E), the computation time is reduced by 0.25 times compared to the C3D20R element (C3D20RE). After that, an experimental processing procedure is performed to evaluate the numerical simulation results. Specifically, the handling of signal noise when measuring a very small displacement at high frequencies of an ultrasonic vibrating device. Based on the confirmed finite element model, this model is extended to evaluate the influence of the load on the amplitude and resonant frequency of the ultrasonic welding system. The results show that when the load increases, the amplitude decreases while the resonant frequency increases. The results of this study can be applied to the design of ultrasonic vibration systems.

Keywords: finite element, ultrasonic transducer, resonance frequency, amplitude, vibration

1 INTRODUCTION

Nowadays, the ultrasonic vibrating device is more and more widely used in life and engineering applications [1–10]. A high-power ultrasonic system usually consists of a transducer, a booster, and a horn. In ultrasonic vibration systems, the transducer acts as the source of the ultrasonic vibration, and it is generally commercial equipment. Pairing the transducer with other components such as the horn and/or booster may change the expected resonant frequency. Several studies have been implemented to evaluate the system response when adding different components to the transducer. Xuan Li et al [11] have modified the ultrasonic vibration device for rock drilling systems that require a small size but very high working performance. Based on the design of the existing Langevin transducer, Mathieson Andrew succeeded in modifying the design parameters to create an ultrasound device suitable for use in bone surgery [2]. In addition, there are other studies [12–17] that also focus on the design of ultrasonic transducers for different purposes. The method of designing a new transducer has traditionally been based on trial and error, thus requiring faster and more reliable tools. The finite element method is usually employed to analyze the system response, where the transducer is often considered the ideal source, providing a preset vibration. Although the piezoelectric part plays an important role in ultrasonic systems, the piezo's electromechanical properties have not been fully considered. Therefore, to get more accurate results, it is necessary to develop a finite element model which describes all parts of the system. Finite element analysis is a very important step in the product design process. It has been widely applied in ultrasonic device analysis. Hassan Al-Budairi et al [18] used finite element analysis to optimize the mechanical structure of longitudinal torsional ultrasonic transducer. Mohamed Y.Baraya [19] used FEM to support the design of the Langevin transducer used in the electromechanical system for measuring the error between finite element analysis and experiment less than 8%. In the process of performing finite element analysis, the choice of mesh size and element type is very important [20] because it directly affects the accuracy of the results and the running time of the model. However, most of the published studies involving ultrasonic devices use only a single element type for components with different electrical and mechanical properties [5,21–26] or the publication is not presented in detail [18,19,27–29]. For example, Ceramic has special electromechanical properties that are different from other transducer components, as well as metal parts of horns, boosters, etc. This leads to the need to use separate elements when analyzing and designing. Furthermore, no benchmark results for the piezoelectric element, in the finite element modeling, have been found in the literature. On the other hand, the accuracy of numerical simulation results, in published results, is often not provided with sufficient accuracy. Therefore, it is very necessary to use different meshing methods and choose different element types for different components. Besides, the experimental results to verify the simulation results are not published in detail and clearly[5,6,25,30–34]

In this paper, a full finite element model is proposed. Accordingly, elements C3D8E and C3D20RE are used for PZT rings, and elements C3D8 and C3D20R are used for other parts of the model. At the same time, the selection of proper element mesh size as well as the calculation of input parameters for the finite element model are also studied. Simulation results are then experimentally validated. Next, the verified model is extended to study the effect of load on the system response. Besides, method of processing experimental data is explained in detail. Since the ultrasonic vibration is of very high frequencies with tiny amplitude, the obtained signals must be filtered with proper method to

obtain reliable data. In our experiments, Philtec RC-19 measuring instrument was employed, providing a cost-effective solution.

The article is divided into four parts: An introduction, an overview of research issues, and the remaining issues that need to be resolved. Material and method section, presenting a new approach to solve existing issues in finite element models and experimental measurement of vibration amplitudes. Results and discussions section, evaluate and confirm the obtained results and extend the finite element model to study other issues. The final section is the conclusions. The new approach in this paper will thoroughly solve the issues related to the finite element model of the ultrasonic vibrating device.

2 MATERIAL AND METHOD

2.1 Material

In this study, a common ultrasonic vibration system, which includes all components such as the transducer and booster, was selected as an object-to-be-tested. A commercial ultrasonic transducer Herrmann Ultrasonic-Ultraschall, having resonant frequency of 20 kHz, paired with a booster, was used. The detail dimension of such device is shown in Fig.1. The device parameters are represented in Table 1 and Table 2.

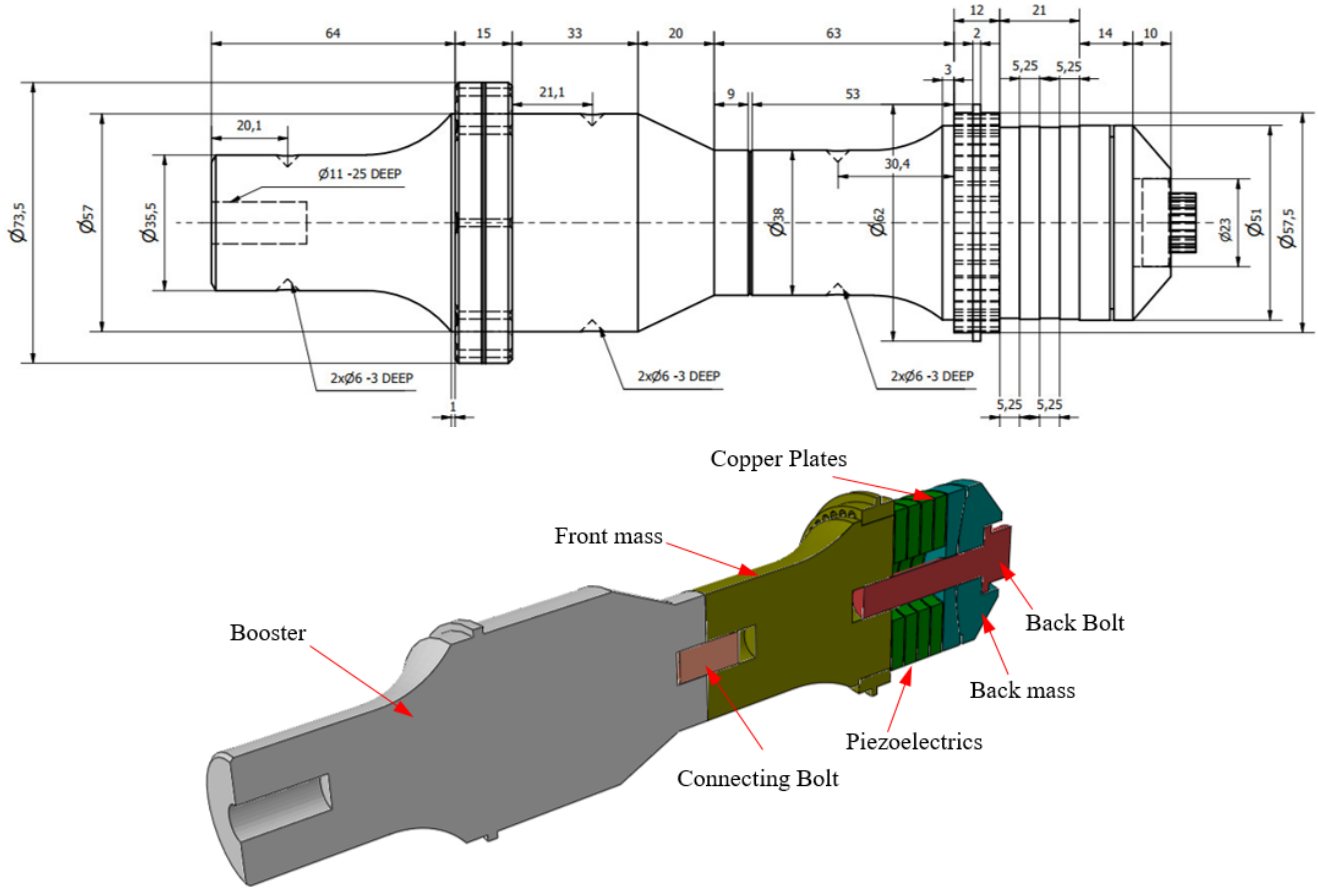

Fig. 1. Ultrasonic transducer and booster (all dimensions are in mm)

Table 1. Parameters of the ultrasonic transducer

Contents	Unit	Specifications
Frequency	kHz	20
Power	W	4000
Ceramic diameter	mm	50
Ceramic rings	-	4
Amplitude	μm	10

Table 2. Booster's material properties

Parameter	Unit	Value
Young's modulus	GPa	200
Density	Kg/m^3	7850
Poisson's ratio	-	0.3
Amplification factor	-	2

2.2 Research Method

The finite element model developed in this paper uses two different types of elements for mechanical and electromechanical properties of the system. Abaqus software was selected to provide the simulation results. First, a modal analysis was performed to find the natural frequency of the ultrasonic vibrator. In this step, a conversion process was made to convert parameters provided by the manufacturer into proper input data in Abaqus software. Then, characteristics such as resonant frequency, and amplitude are determined. Finally, the results of the FEM model are tested and validated.

Firstly, the basic properties of the PZT ring are introduced. The PZT rings are made from materials with piezoelectric properties. Accordingly, linear piezoelectric properties are the combined effect of electromechanical and elastic behavior. The linear electrical behavior of the material can be expressed in the following form:

$$D = \varepsilon E \tag{1}$$

Where, D is the electric charge density displacement, ε is permittivity, E is electric field strength. The Hooke's law for elastic materials:

$$S = sT \tag{2}$$

Where, S is strain, s is compliance under short-circuit conditions, T is stress. These relationships are expressed as coupling equations, where the strain-charge form is:

$$\begin{aligned} S &= sT + d^t E \\ D &= dT + \varepsilon E \end{aligned} \tag{3}$$

Where, d is matrix for the direct piezoelectric effect. The piezoelectric coefficients can be defined as follows:

$$d_{ij} = \left(\frac{\partial D_i}{\partial T_j}\right)^E = \left(\frac{\partial S_i}{\partial E_j}\right)^T ; e_{ij} = \left(\frac{\partial D_i}{\partial S_j}\right)^E = -\left(\frac{\partial T_j}{\partial E_i}\right)^T ; g_{ij} = -\left(\frac{\partial E_i}{\partial T_j}\right)^D = \left(\frac{\partial S_j}{\partial D_i}\right)^T ; h_{ij} = \left(\frac{\partial E_i}{\partial S_j}\right)^D = -\left(\frac{\partial T_j}{\partial D_i}\right)^S \tag{4}$$

Relationships between electrical and elastic mechanical behavior.

Strain – Charge Form:

$$S = s_E T + d^t E; D = d.T + \varepsilon_T E \tag{5}$$

Stress- Charge Form

$$T = c_E S - e^t E; D = e.S + \varepsilon_s E \tag{6}$$

Strain-Voltage Form:

$$S = s_D T + g^t D; E = -g.T + \varepsilon_T^{-1} D \tag{7}$$

Stress – Voltage Form:

$$T = c_D S - q^t D; E = -q.S + \varepsilon_S^{-1} D \tag{8}$$

In ultrasonic transducers, the piezo ceramic ring has the main function in conversion electrical energy into mechanical energy. Therefore, the analysis of piezoelectric materials requires full consideration of their mechanical, electromechanical, and electrical aspects. These are very important parameters that have the greatest influence on the numerical simulation results. However, in the published ultrasonic vibration device simulation studies, most of the system behavior is obtained as a result of using a single element with mechanical properties for the entire model including the PZT material. In this study, the authors will use a piezoelectric element as excitation resource. To provide the PZT parameters for the simulation model, it is necessary to convert the data provided from the manufacturer in the form the constant stress. The conversion of stress to a dielectric constant at a constant strain $\left[\varepsilon^S\right]$ can be made using the following relationship:

$$\left[\varepsilon^S\right] = \left[\varepsilon^T\right] - \left[e\right]^t \left[d\right] \tag{9}$$

Where $\left[e\right]^t$ and $\left[d\right]$ are the transpose of the charge constants matrix in the stress form and the charge constants matrix in the strain form, respectively. According to Equation 9, the linear relationship between the mechanical and electrical fields in the matrix is provided in Abaqus:

$$\left[d\right] = \begin{bmatrix} d_{1\,11} & d_{1\,22} & d_{1\,33} & d_{1\,12} & d_{1\,13} & d_{1\,14} \\ d_{2\,11} & d_{2\,22} & d_{2\,33} & d_{2\,12} & d_{2\,13} & d_{2\,14} \\ d_{3\,11} & d_{3\,22} & d_{3\,33} & d_{3\,12} & d_{3\,13} & d_{3\,14} \end{bmatrix} \tag{10}$$

$$\left[e\right] = \begin{bmatrix} e_{1\,11} & e_{1\,22} & e_{1\,33} & e_{1\,12} & e_{1\,13} & e_{1\,14} \\ e_{2\,11} & e_{2\,22} & e_{2\,33} & e_{2\,12} & e_{2\,13} & e_{2\,14} \\ e_{3\,11} & e_{3\,22} & e_{3\,33} & e_{3\,12} & e_{3\,13} & e_{3\,14} \end{bmatrix} \tag{11}$$

Where $d_{1\,23}$, $d_{2\,13}$, $d_{3\,11}$, $d_{3\,22}$, and $d_{3\,33}$ are provided by the manufacturer. Besides, the constant piezoelectric charge [e] is also calculated according to the formula 12 [35].

$$[e]=[d][D] \tag{12}$$

With D_{ijkl} is a fourth-order elastic tensor of the elastic stiffness parameter evaluated at a constant electric field

$$[D]=\begin{bmatrix} D_{1111} & D_{1122} & D_{1133} & 0 & 0 & 0 \\ & D_{2222} & D_{2233} & 0 & 0 & 0 \\ & & D_{3333} & 0 & 0 & 0 \\ & & & D_{1212} & 0 & 0 \\ & symmetric & & & D_{1313} & 0 \\ & & & & & D_{2323} \end{bmatrix} \tag{13}$$

$$D_{1111}=E_1(1-\nu_{23}\nu_{32})\gamma; D_{1122}=E_2(\nu_{12}-\nu_{32}\nu_{13})\gamma; D_{1133}=E_3(\nu_{13}-\nu_{12}\nu_{23})\gamma; D_{2222}=E_2(1-\nu_{13}\nu_{31})\gamma; \tag{14}$$

$$D_{2233}=E_3(\nu_{23}-\nu_{21}\nu_{13})\gamma; D_{3333}=E_3(1-\nu_{12}\nu_{21})\gamma; D_{1212}=G_{12}; D_{1313}=G_{13}; D_{2323}=G_{23} \tag{15}$$

$$\gamma=\frac{1}{1-\nu_{12}\nu_{21}-\nu_{23}\nu_{32}-\nu_{31}\nu_{13}-2\nu_{21}\nu_{32}\nu_{13}} \tag{16}$$

The values provided by the manufacturer, for the material PZT-8, are shown in Table 3. The main steps to calculate the input parameter value for the finite element model in Abaqus according to the formulas (3), (9), and (13). When calculating the data to input in Abaqus, equation (10) and equation (11) degenerate into:

$$[d]=\begin{bmatrix} 0 & 0 & 0 & 0 & 0 & d_{1\,23} \\ 0 & 0 & 0 & 0 & d_{2\,13} & 0 \\ d_{3\,11} & d_{3\,22} & d_{3\,33} & 0 & 0 & 0 \end{bmatrix} \tag{17}$$

$$[e]=\begin{bmatrix} 0 & 0 & 0 & 0 & 0 & e_{1\,23} \\ 0 & 0 & 0 & 0 & e_{2\,13} & 0 \\ e_{3\,11} & e_{3\,22} & e_{3\,33} & 0 & 0 & 0 \end{bmatrix} \tag{18}$$

The obtained results are shown in Table 4, Table 5, and Table 6.

Table 3. Values of PZT provided by the manufacturer

E_{11} (m^2/N)	E_{22} (m^2/N)	E_{33} (m^2/N)	E_{12} (m^2/N)	E_{13} (m^2/N)	ν_{13}	ν_{23}
1.0E-11	1.0E-11	8.50E-12	-4.50E-12	-2.5E-12	3.0E-01	3.0E-01
d_{33} (C/N)	d_{31} (C/N)	d_{15} (C/N)	$\varepsilon^s_{33}/\varepsilon_0$	$\varepsilon^s_{11}/\varepsilon_0$	ε_0 (F/m)	
2.25E-10	-3.70E-11	3.30E-10	3.65E-10	0.0E+00	-9.5E-11	

Table 4. Piezoelectric elastic properties of material

D_{1111} (N/m^2)	D_{1122} (N/m^2)	D_{1133} (N/m^2)	D_{2233} (N/m^2)	D_{3333} (N/m^2)
9.22E+10	-6.75E+09	2.58E+10	2.58E+10	8.59E+10
D_{1212} (N/m^2)	D_{1313} (N/m^2)	D_{2323} (N/m^2)	D_{2222} (N/m^2)	
4.65E+10	4.65E+10	4.65E+10	9.34E+10	

Table 5. Charge constants matrix in the strain of material (unit is C/N)

$d_{1\,11}$	$d_{1\,22}$	$d_{1\,33}$	$d_{1\,12}$	$d_{1\,13}$	$d_{1\,23}$	$d_{2\,11}$	$d_{2\,22}$	$d_{2\,33}$
0.0E+00	0.0E+00	0.0E+00	0.0E+00	0.0E+00	3.65E-10	0.0E+00	0.0E+00	0.0E+00
$d_{2\,12}$	$d_{2\,13}$	$d_{2\,23}$	$d_{3\,11}$	$d_{3\,22}$	$d_{3\,33}$	$d_{3\,12}$	$d_{3\,13}$	$d_{3\,23}$
0.0E+00	3.65E-10	0.0E+00	-9.5E-11	-9.5E-11	2.35E-10	0.0E+00	0.0E+00	0.0E+00

Table 6. Piezoelectric charge of material (unit is C/N)

$e_{1\,11}$	$e_{1\,22}$	$e_{1\,33}$	$e_{1\,12}$	$e_{1\,13}$	$e_{1\,23}$	$e_{2\,11}$	$e_{2\,22}$	$e_{2\,33}$
0.0E+00	0.0E+00	0.0E+00	0.0E+00	0.0E+00	1.67E+01	0.0E+00	0.0E+00	0.0E+00
$e_{2\,12}$	$e_{2\,13}$	$e_{2\,23}$	$e_{3\,11}$	$e_{3\,22}$	$e_{3\,33}$	$e_{3\,12}$	$e_{3\,13}$	$e_{3\,23}$
0.0E+00	1.67e+01	0.0E+00	-1.97E+00	-1.97E+00	1.570E+01	0.0E+00	0.0E+00	0.0E+00

As mentioned above, choosing the right element for the finite element model is very necessary. The 8-node element (C3D8,C3D8E) and the 20-node element (C3D20R, C3D20RE) both have mechanical properties but the element C3D8E and C3D20RE has additional electrical properties. Therefore, in each research FEM model, the corresponding element used are (C3D8, C3D8E) and (C3D20R, C3D20RE). At the same time, the authors solved the model on progressively finer meshes and compared the results (mesh size 1, 2, 3, and 4 mm). The finite element 3D model of the experimental ultrasound device was developed to accurately predict device responses as shown in Fig. 2. The simulations are performed on computers with configuration: Processor Intel(R) Xeon(R) CPU E5-2689 0 @ 2.60GHz 2.60 GHz, RAM 32.0 GB.

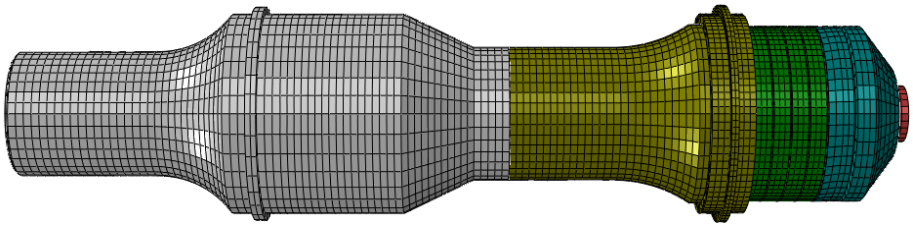

Fig. 2. Finite element 3D model of ultrasonic vibrating device

3 RESULTS AND DISCUSSIONS

3.1 Simulation Results

For simulation with element C3D8 and C3D8E, a numerical simulation is performed to determine the natural frequency and mode of vibration. The obtained results show that the transducer has bending vibration at 17420 Hz and 22662 Hz, torsional vibration at 1888 Hz, and longitudinal vibration at 19703 Hz (Fig. 3). Numerical harmonic analysis is also used to evaluate the vibration amplitude and resonance frequency when operating the device. The result of harmonic analysis is shown in Fig.4. Accordingly, the vibration amplitude at the end of the booster is 19.1 µm, corresponding to the resonant frequency of 19703 kHz.

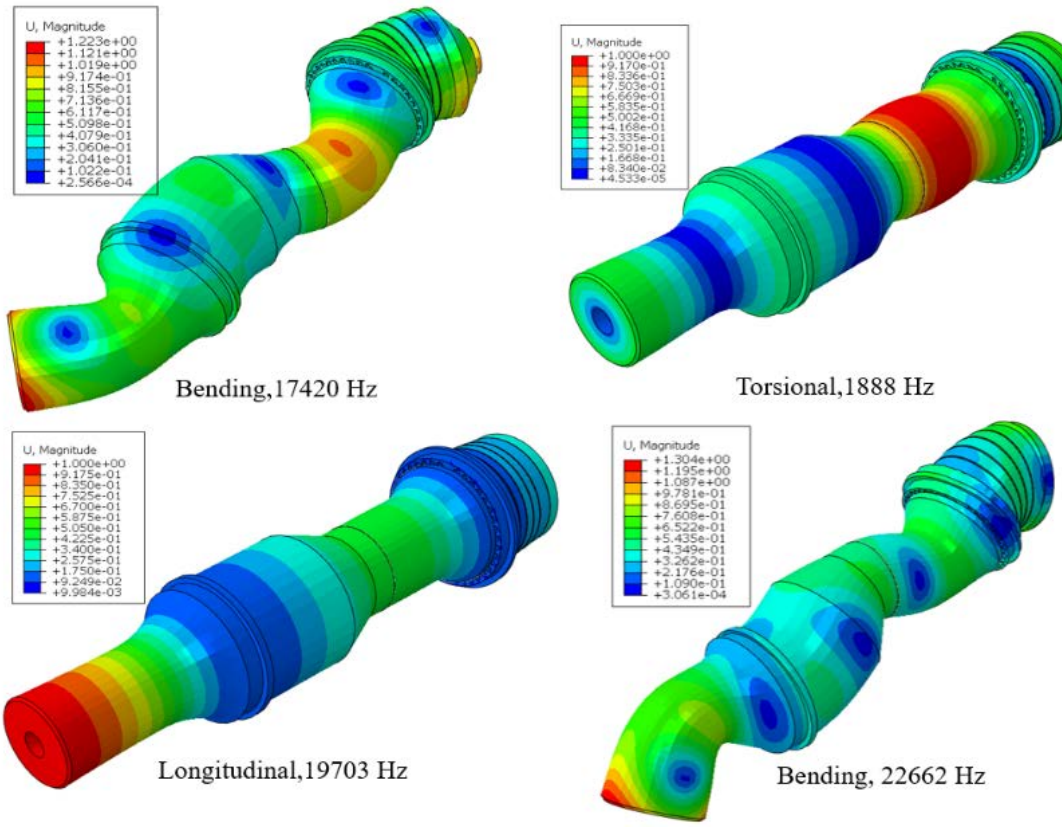

Fig.3. Mode and natural frequency of ultrasonic vibration device (mesh size 2 mm)

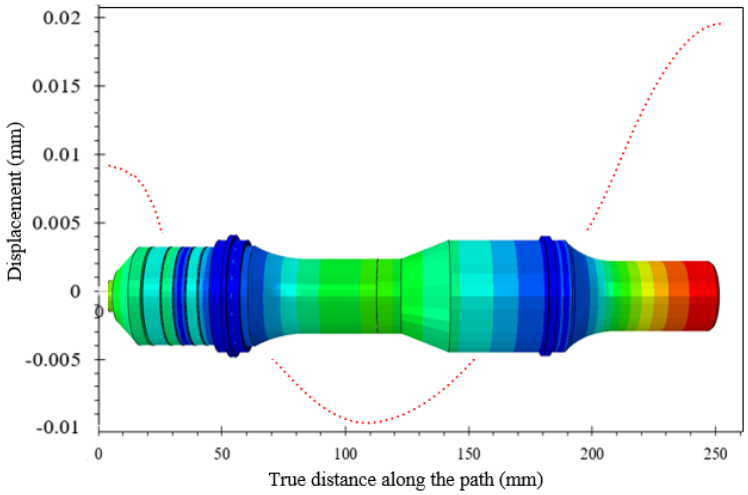

Fig. 4. Vibration amplitude of the ultrasonic transducer (mesh size 2mm)

The meshing and use of the appropriate element type have a great influence on the results as well as the CPU time in numerical simulation. A small mesh will lead to a more precise solution. However, as the mesh is made smaller, the computation time increases and requires a large computer configuration. In this study, mesh sizes are analyzed and compared based on ensuring accuracy and requiring reasonable running time. Therefore, to study the evaluation of resonant frequency, ultrasonic vibration amplitude as well as running time, it is necessary to perform numerical simulation with four mesh refinements (mesh size 1, 2, 3 and 4mm). Effect of mesh refinement on the resonance frequency and amplitude is shown in the Fig. 5. The received resonance frequency responses tend to be similar for the four meshes, but the amplitudes are different for the mesh sizes.

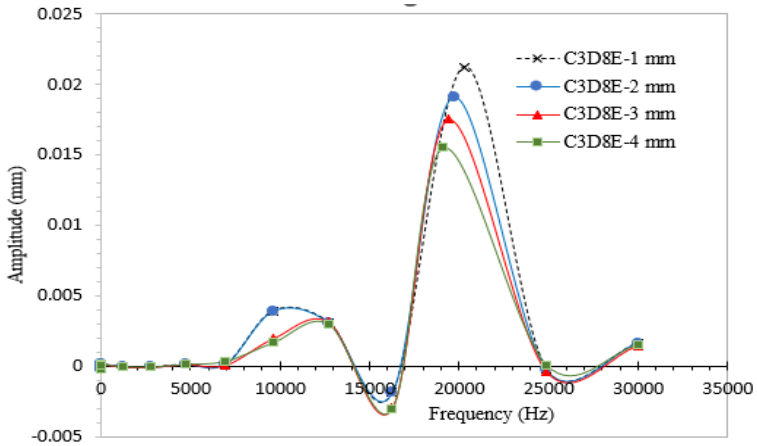

Fig. 5. Effect of mesh refinement on resonance frequency and amplitude

After conducting a series of simulations with four different mesh sizes, different model energy plots for the four meshes are plotted in Fig.6. When doing the kinematics calculation, the kinetic energy changes with the frequency as shown in Fig. 6a. The energy balance for the four meshes with time (Fig. 6b). It is easy to see that in the numerical model this value is only approximately constant, with an error of less than 1%. After analyzing this sensitivity, a mesh size of 2 mm was selected for the calculations involved while keeping the computational cost reasonable.

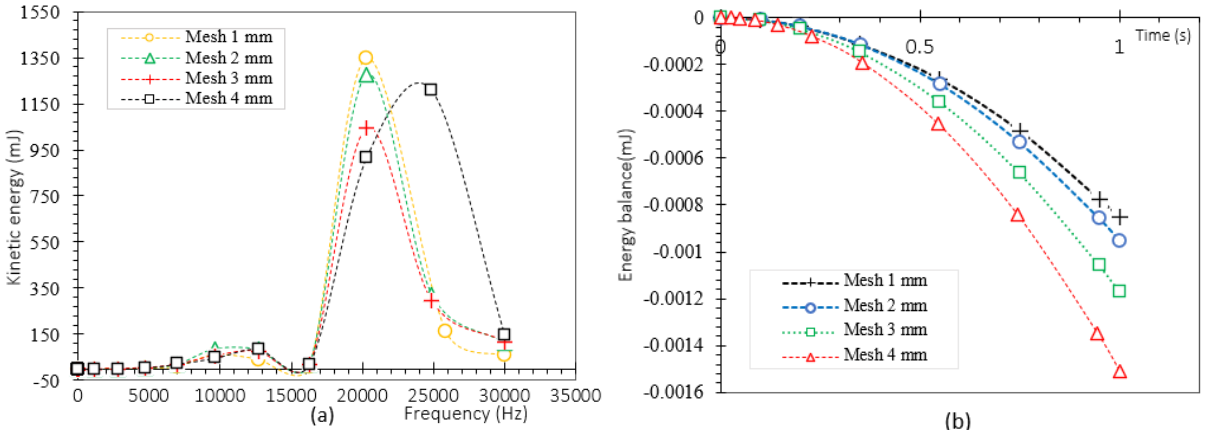

Fig. 6. Effect of mesh size on various model energies: (a) Kinetic energy, (b) Energy Balance

For the element C3D20R (C3D20RE), a series of numerical simulations are performed similarly to the element C3D8 (C3D8E). A comparison of the results between these two elements is shown in Table 7 and Fig. 7. It shows the change of resonant frequency, oscillation amplitude as well as running time, corresponding to different mesh sizes, for the two element types. It is easy to see that the running time when using the C3D20R element (C3D20RE) is much larger than when using the C3D8 element (C3D8E). The difference in running time is due to the element mesh used for piezoelectric materials. Specifically, there is a difference in electric potential at the actuator and sensor monitor point between linear element mesh C3D8E and Quadratic Reduced Integration mesh C3D20RE elements.

Table 7. Effect of mesh size and element style

Element Type	Mesh size (mm)	Number of Elements	Resonant Frequency (Hz)	Amplitude (mm)	Time CPU (s)
C3D8 (C3D8E)	1	398238	20303	0.022	43768
	2	126694	19703	0.0191	16320
	3	50658	19406	0.0175	3720
	4	25320	19121	0.0155	1860
C3D20R (C3D20RE)	1	398238	20613	0.0214	54710
	2	126694	19871	0.0195	20456
	3	50658	19566	0.0185	4650
	4	25320	19281	0.0159	2325

On the other hand, the first-order elements are computationally efficient and improve contact convergence. However, if the mesh size is large, the element will become stiff, reducing the accuracy of the results. As the mesh size decreases, the effect of this problem becomes negligible. The quadratic elements have more accurate results, and better fit for complex models but the model computation time will be longer. As can be seen from Table 7 and Fig. 7, the recommendation to select the element type for the finite element model requires selecting elements with similar properties such as C3D8 and C3D8E or C3D20R and C3D20RE. Using the mesh size of 2 mm, the running time for the C3D20R (C3D20RE) element is 1.25 times that of the C3D8 (C3D8E) element.

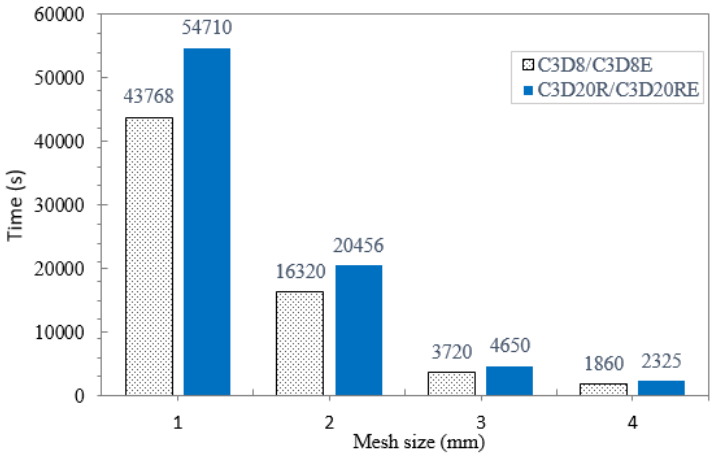

Fig. 7. Comparative computation time between two element types

3.2 Experimental Study and Discussion

3.2.1 Experimental setup and data processing

Experiments were implemented to verify the results of finite element analysis such as frequency measurement, amplitude measurement to compare with simulation results. The first basis of the measurement experiment is the determination of the resonant frequency. The resonant frequency of the ultrasonic vibration device is a very important specification. Therefore, to fabricate a complete ultrasonic vibration system as well as to apply existing systems in practice, it is necessary to check this parameter first. Based on related studies [13,36-39], the authors determine the principle of determining the impedance and resonance frequency. This principle will be used in the measurement procedure to determine the amplitude of oscillations at the resonant frequency of the ultrasonic vibration system in this study. The obtained measurement result is shown in Fig. 8. The resonant and anti-resonant frequencies obtained are correct with the values given by the designer. Hence, the electromechanical coupling coefficient, the conversion efficiency between electrical energy and acoustic energy in PZT, is guaranteed [40].

To measure very small mechanical displacements (μm), an RC-19 displacement sensor is used. This is a reflective type of detector based on detecting the intensity of the reflected light. The model RC sensor has a pair of fiber detectors in the sensor head. Light reflected off the target follows two separate paths back to the electronics, where scaling provides a distance measurement independent of different surface reflectance. RC-type fiber optic sensor is a family of very high-performance non-contact displacement sensors with resolutions down to 0.01μm and analog output from 0 to 5 Volts. In this study, an ultrasonic power supply (Series welding, output power 3000W and mains supply 220V, 50-60 Hz) is used. It is compatible and easily modifiable to drive almost any piezoelectric ultrasonic

transducer presently used, operating up to 100 kHz (digital software settings, easy frequency selection in any range, and easy frequency window selection in any range). In addition, to conduct this research, it is necessary to use supporting devices such as Jig, DAQ kits, as well as the help of express acquisition software Signal Express, data analysis software OriginLab.

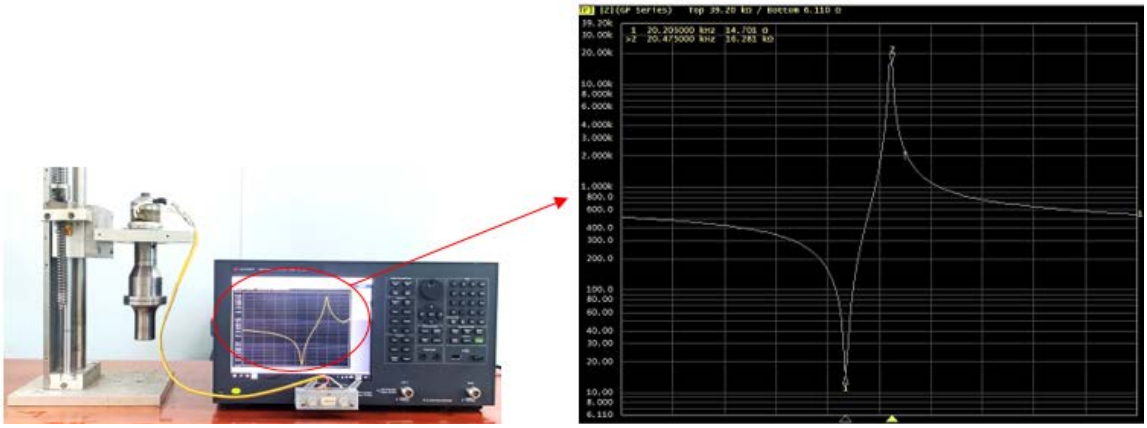

Fig. 8. Determine the impedance and resonance frequency of the ultrasonic vibration device

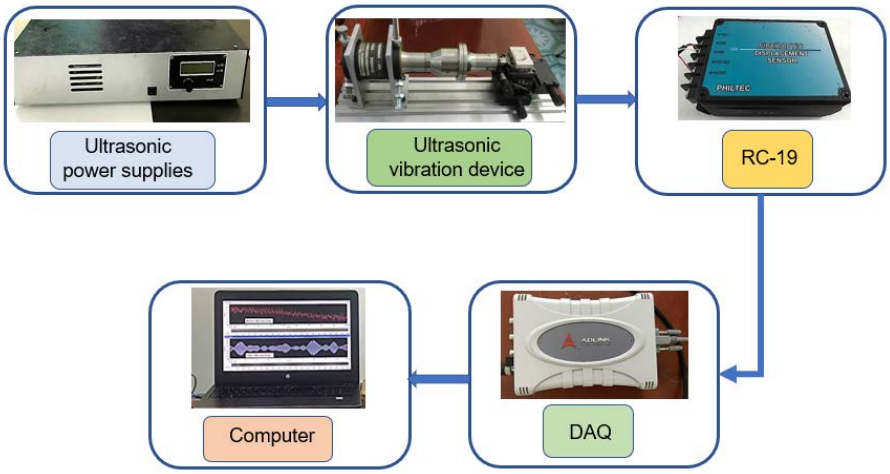

Fig. 9. Experimental set-up for the vibration amplitude measurement

An experimental system to measure the amplitude of the ultrasonic transducer is set up as shown in Fig. 9. It consists of an ultrasonic vibration system: An ultrasonic generator, an ultrasonic transducer, and booster; Optical measuring system: the RC-19 displacement sensor and the controller (Philtec RC-19 is an instrument used to measure the distance, displacement, and vibration of small targets > Ø 0.5 mm with high resolution [41]), and a data acquisition system. The ultrasonic vibrator is mounted on a jig and clamped at a position where the vibration amplitude (displacement) is zero. The ultrasonic generator converts 50Hz power to ultrasonic frequency AC output. The signal is fed to a piezoelectric transducer inside the ultrasonic vibration which converted the signal to mechanical vibrations. The RC-19 optical cable and custom sensor head are installed as shown in Fig.10 (The sensor head is set up to measure at four different positions). Adjust the gap between the sensor and the booster head so that: The sensor is perpendicular to the target and gapped to its range of highest sensitivity. Calibration is provided for the sensor giving the voltage output response to distance. Within the bounds of the linear range, convert the change in voltage output as follows:

$$Distance\ (\mu m) = \Delta\ millivolts \div Sensitivity \tag{19}$$

The scanning frequency of the ultrasonic power supply is adjusted in the range of 19 kHz – 21 kHz. In this way, the values can be scanned to get the most appropriate ultrasonic load range. Measurement data is recorded by using Signal Express software. This data is analyzed with the help of Origin Lab software to find the amplitude of the transducer system. A very important note: When conducting measurement experiments, the authors discovered the existence of some strange signals causing amplitude noise. To solve this issue, a digital filter was used to remove these noisy frequencies. The distribution of voltage in real-time is shown as shown in Fig.11 and Fig.12. It clearly shows the effect of noise on the vibration amplitude of the equipment used in this study. Before noise filtering, the voltage amplitude is unevenly distributed, which makes it difficult to accurately determine the amplitude to be measured (Fig.11). After using the noise filtering method, the received amplitude is distributed according to the rule, so it is easy to accurately determine the amplitude to be measured (Fig.12). Based on this obtained data, the fast Fourier transform (FFT) algorithm is used and combined with voltage conversion relationship and measurement sensitivity in equation 15, to determine the resonant frequency and amplitude of oscillation. The result obtained is

illustrated in Fig. 13. It is easy to see that the largest amplitude of vibration measured is 20.07 µm, corresponding to the resonant frequency 20053.29 Hz.

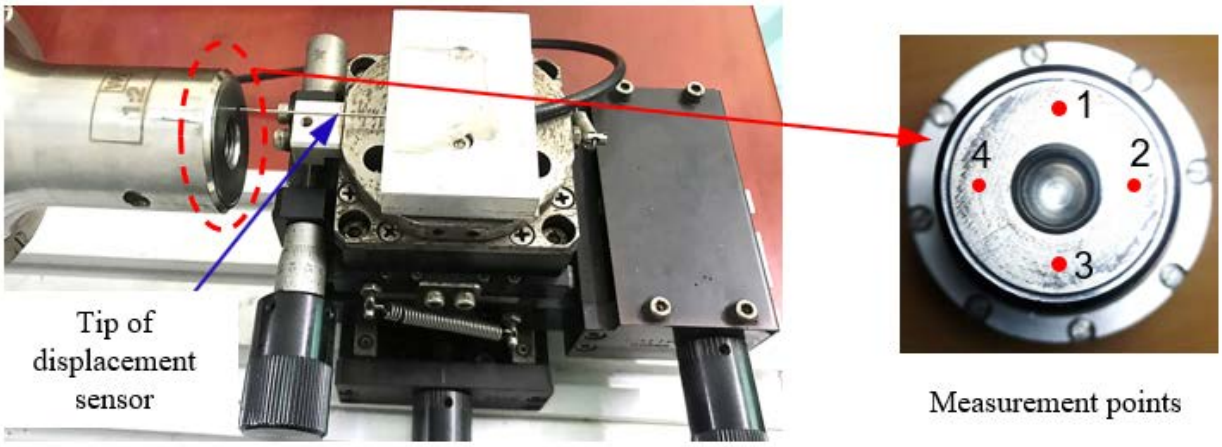

Fig. 10. Install sensor head for displacement measurement

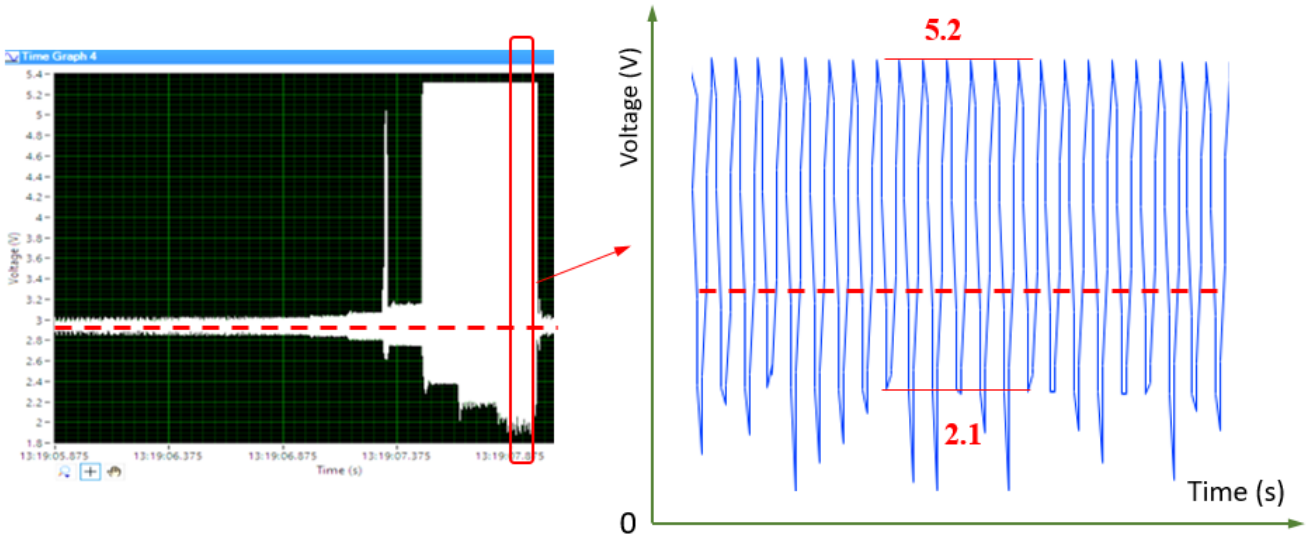

Fig. 11. Measurement results before noise filtering

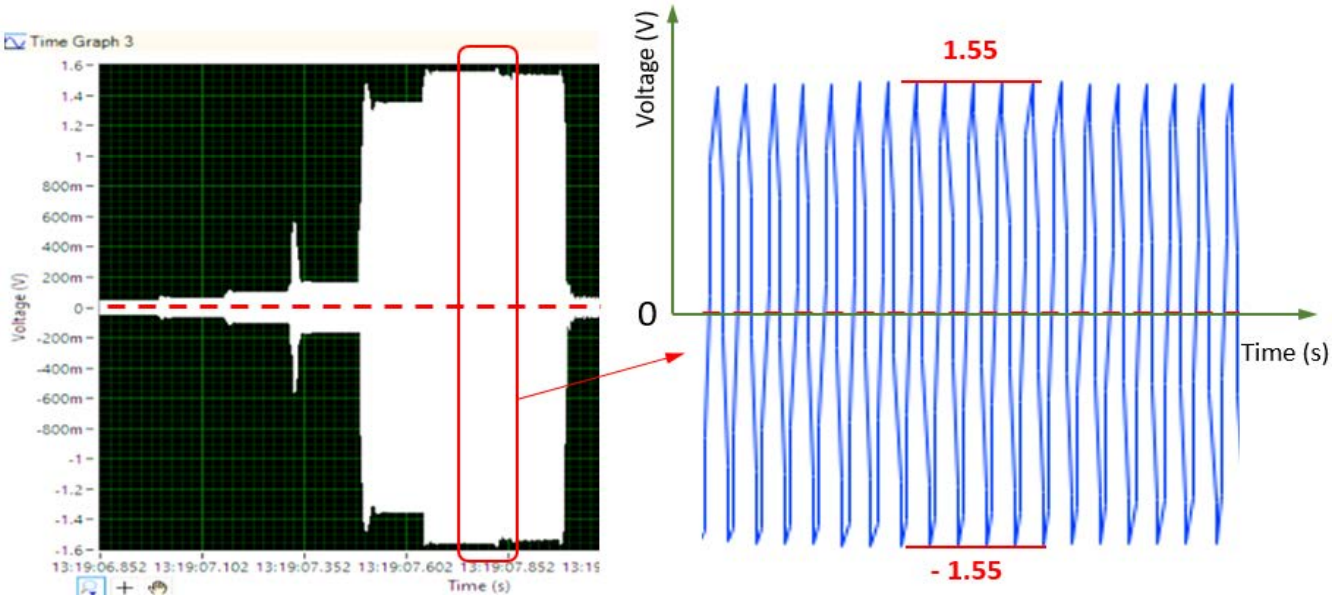

Fig. 12. Measurement results after noise filtering

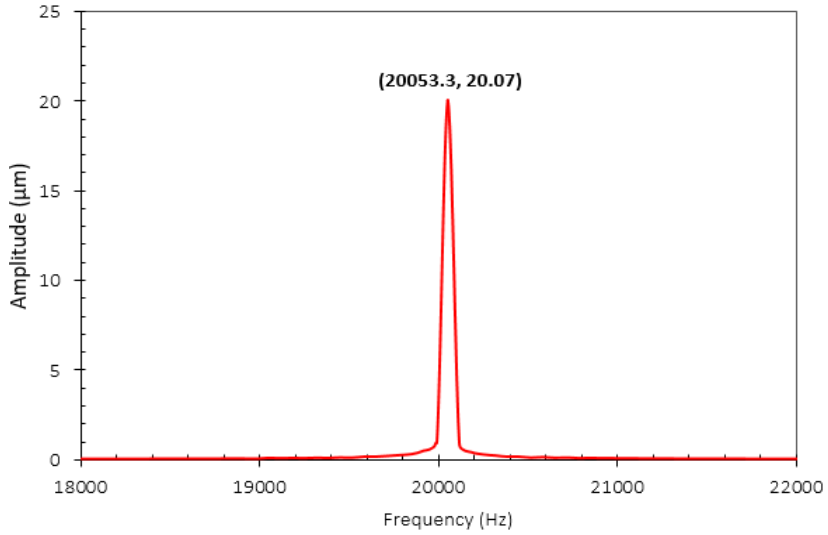

Fig. 13. Resonance frequency vs amplitude received after performing FFT

3.2.2 Validate the finite element model

The results of the experimental procedure established in this study show that the values of the quantities to be measured are consistent with the design values. Specifically, the measured resonant frequency is 20.053 kHz, corresponding to 20.07 µm amplitude compared to 20 kHz and 20 µm design values. However, to evaluate the results of the measurement process comprehensively, it is necessary to compare with the numerical simulation results for the conducted experiment. The comparison of numerical and experimental simulation results is shown in Table 8. The resonant frequency error is 1.7% and the vibration amplitude error is 4.83%. The numerical results obtained are in good agreement with the experimental results. On the other hand, the numerical simulation results in the previous section indicate that the displacements of the points on the booster head are the same (Fig.14). That once again confirms the reliability of the model and the numerical simulation results performed.

Table 8. The comparison of numerical and experimental simulation results

	Experiment	Simulation	Erros (%)
Resonant frequency (Hz)	20053	19703	1.74
Vibration amplitude (µm)	20.07	19.10	4.83

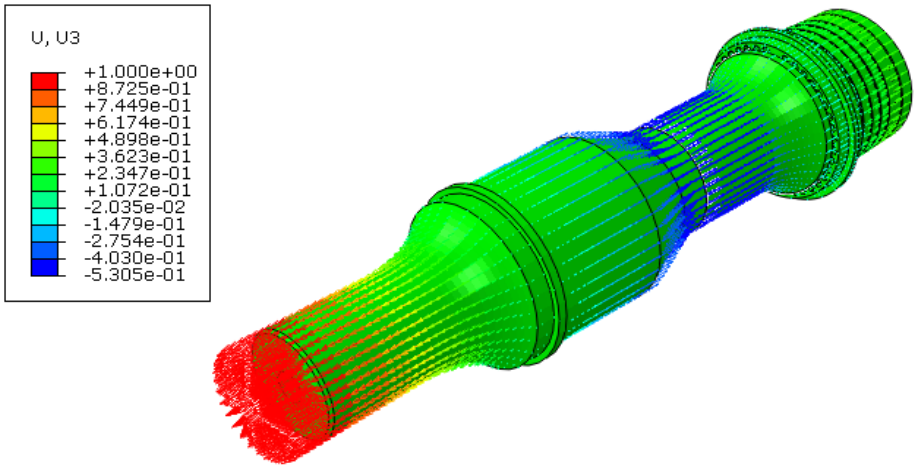

Fig. 14. The displacement of the points on the top of the booster

3.3 Effect of force on device characteristics

Based on the comparison of results between the experiment and simulation, the authors continue to study the change of amplitude and resonance frequency of this device, when applied force, by finite element analysis method. The purpose of this analysis is to find out the change rule of the resonant frequency and amplitude of the ultrasonic vibrating device after the applied load (Fig. 15). The actual welding force is divided into different values to simulate the change in resonant frequency and amplitude. After the system was loaded during actual processing, the effects of different force loads were accurately analyzed. According to the actual welding force during work, the axial pressure 0–250 N is gradually applied to the device, and the solution order is set to 5 steps. The changes in the resonance frequency and amplitude of the system are shown in Fig. 16. Fig. 16a shows the decrease in the amplitude of vibration when force is applied. As the force increases, the amplitude decreases. At this time, the efficiency of

converting electrical energy into mechanical energy decreases, which seriously affects the capacity and stability of the system. Therefore, it is necessary to calculate to compensate for this energy loss. In Fig. 16b, the simulation results showed that the resonant frequency of the device changes with increasing direction, but the range of change is small. Since the device works in the elastic phase, the resonant frequency does not change significantly.

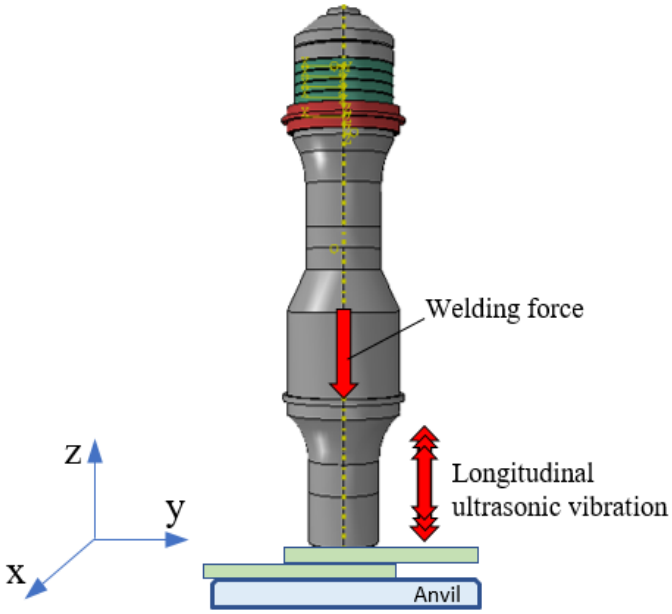

Fig. 15. Forces acting on the device and specimen during welding

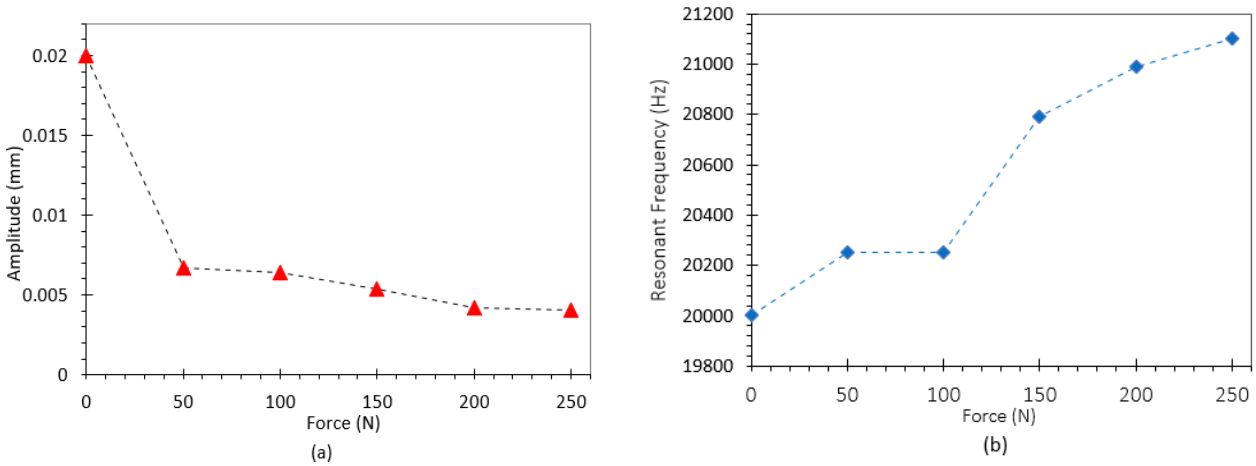

Fig. 16. Effect of force on resonance amplitude (a), and frequency (b)

4 CONCLUSION

This study has solved some outstanding issues related to ultrasonic vibration equipment. By new approach, the authors have successfully built a finite element model of an ultrasonic vibrating device with full properties of the real model. In addition to the basic elements for solid modeling (C3D8, C3D20R), piezoelectric elements C3D8E and C3D20RE for ceramic materials are also used. The process of calculating the parameters for piezoelectric materials as well as the selection of the mesh size to increase the convergence and reduce the running time is also mentioned in this study. Besides, a detailed procedure for measuring vibration amplitude and resonance frequency is also determined in this study. The correctness of the finite element model is confirmed by comparing experimental and simulation results. Finally, based on the obtained results, the effect of welding force on the performance of ultrasonic welding equipment continues to be studied by the finite element analysis method.

5 ACKNOWLEDGMENTS

This work was funded by the Ministry of Education & Training Vietnam (grant number B2020-TNA-02)

6 REFERENCES

[1] B. Chandra Behera (2011), Development and Experimental Study of Machining Parameters in Ultrasonic Vibration-assisted Turning,

fromhttp://ethesis.nitrkl.ac.in/4416/1/Development_and_experimental_study_of_machining_parameters_in_ultrasonic_vibration-assisted_turning.pdf

[2] A. C. Mathieson (2012), Nonlinear Characterisation Of Power Ultrasonic Devices Used In Bone Surgery, from http://theses.gla.ac.uk/3135/.

[3] X. Li, P. Harkness, K. Worrall, R. Timoney, and M. Lucas (2017) A Parametric Study for the Design of an Optimized Ultrasonic Percussive Planetary Drill Tool, IEEE Trans. Ultrason. Ferroelectr. Freq. Control, vol. 64, no. 3, pp. 577–589, DOI: 10.1109/TUFFC.2016.2633319.

[4] Y. Yao, Y. Pan, and S. Liu (2020), Power ultrasound and its applications: A state-of-the-art review, Ultrason. Sonochem., vol. 62, DOI: 10.1016/j.ultsonch.2019.104722

[5] A. T. São-carlense, S. Carlos, S. P. Brazil, and D. Vandepitte (2007), Experimental and Finite Element Analysis of Composite, pp. 447–450

[6] M. Rezaei, M. Farzin, F. Ahmadi, and M. R. Niroomand, Design (2022), Analysis and Manufacturing of a Bone Cutting Ultrasonic Horn-Tool and Verification with Experimental Tests, Journal of Applied and Computational Mechanics, vol. 8, no. 2. 2022, 438–447, DOI: 10.22055/jacm.2020.31298.1904.

[7] O. N. Arani, A. Yaghootian, and S. Sodagar (2022), Investigation on the Crack Effect in the Cylinder and Matrix on the Backscattering Field Frequency Specifications using the Finite Element Method, Journal of Applied and Computational Mechanics, vol. 8, no. 2, pp. 448–455,DOI: 10.22055/jacm.2020.31700.1910

[8] M. Zarei, G. R. Faghani, M. Farzin, and M. Mashayekhi (2017), Investigation on the ultrasonic tube hydroforming in the bulging process using finite element method, Journal of Applied and Computational Mechanics, vol. 3, no. 4, pp. 251–257, DOI: 10.22055/jacm.2017.21852.1119

[9] O. N. Arani, M. Z. Salimabad, A. Yaghootian, and M. Kari (2023), Calculation of Backscattered Ultrasonic Waves Field from a Copper-clad Steel Rod Immersing in Water and Effect of Clad Corrosion and Interfacial Disbond between Clad and Rod Defects on this Field using the Finite Element Method, Journal of Applied and Computational Mechanics, vol. 9, no. 1, pp. 58–71, DOI: 10.22055/jacm.2021.38098.3172.

[10] S. A. Arhamnamazi, N. B. M. Arab, A. R. Oskouei, and F. Aymerich (2019), Accuracy assessment of ultrasonic C-scan and X-ray radiography methods for impact damage detection in glass fiber reinforced polyester composites, J. Appl. Comput. Mech., vol. 5, no. 2, pp. 258–268, DOI: 10.22055/JACM.2018.26297.1318

[11] X. Li, M. Lucas, and P. Harkness (2018), Full and Half-Wavelength Ultrasonic Percussive Drills, IEEE Transactions on Ultrasonics, Ferroelectrics, and Frequency Control, vol. 65, no. 11, pp. 2150–2159, DOI: 10.1109/TUFFC.2018.2867535

[12] D. A. DeAngelis, G. W. Schulze, and K. S. Wong (2015), Optimizing Piezoelectric Stack Preload Bolts in Ultrasonic Transducers, in Physics Procedia, vol. 63, pp. 11–20, DOI: 10.1016/j.phpro.2015.03.003.

[13] M. V. Guiman and I. C. Roca (2017), A New Approach on Vibrating Horns Design, Shock and Vibration, vol. 2017, DOI: 10.1155/2017/8532021.

[14] K. Nakamura (2020), Evaluation methods for materials for power ultrasonic applications, Japanese Journal of Applied Physics, vol. 59, DOI: 10.35848/1347-4065/ab9230

[15] E. Evaluation, O. F. Indicators, O. F. Nonlinearity, F. O. R. Use, I. N (2002). Ultrasound, and T. Characterizations, Experimental Evaluation of Indicators of Nonlinearity, vol. 28, no. 02, pp. 1509–1520

[16] R. Marat-Mendes, C. J. Dias, and J. N. Marat-Mendes (2002), A comparative study of piezoelectric materials using smart angular accelerometers, in Key Engineering Materials, vol. 230–232, pp. 181–184,DOI: 10.4028/www.scientific.net/kem.230-232.181

[17] S. Sherrit, B. P. Dolgin, Y. Bar-Cohen, D. Pal, J. Kroh, and T. Peterson (1999), Modeling of horns for sonic/ultrasonic applications, in Proceedings of the IEEE Ultrasonics Symposium, vol. 1, pp. 647–651, DOI: 10.1109/ultsym.1999.849482

[18] H. Al-Budairi, M. Lucas, and P. Harkness (2013), A design approach for longitudinal–torsional ultrasonic transducers, Sensors Actuators A Phys., vol. 198 , pp. 99–106, DOI: 10.1016/j.sna.2013.04.024.

[19] M. Baraya, Mohamed Y.; Hossam (2020), Design of an electromechanical system for measuring and monitoring micro-ultrasonic amplitude of Langevin transducer, International J. Adv. Manuf. Technol, DOI: 10.1007/s00170-020-04922-w.

[20] V. D. Luong, A. S. Bonnin, F. Abbès, J. B. Nolot, D. Erre, and B. Abbès (2021), Finite Element and Experimental Investigation on the Effect of Repetitive Shock in Corrugated Cardboard Packaging, J. Appl. Comput. Mech., vol. 7, no. 2, pp. 820–830, DOI: 10.22055/jacm.2020.35968.2771

[21] X. Chen, Y. Yin, Q. Hou, L. Jin, and X. Li (2010), The simulation and structural optimization of ultrasonic transducer, 2010 2nd Int. Conf. Ind. Inf. Syst. IIS 2010, vol. 1, pp. 330–333, DOI: 10.1109/INDUSIS.2010.5565844

[22] I. Jovanović, D. Mančić, U. Jovanović, and M. Prokić (2017), A 3D model of new composite ultrasonic transducer, J. Comput. Electron., vol. 16, no. 3, pp. 977–986, DOI: 10.1007/s10825-017-1000-0

[23] Q. Xu, A. Gao, Y. Li, and Y. Jin (2022), Design and Optimization of Piezoelectric Cantilever Beam Vibration Energy Harvester, Micromachines, vol. 13, no. 5, DOI: 10.3390/mi13050675

[24] M. Liu (2012), Finite Element Analysis of the Contact Deformation of Piezoelectric Materials, Theses and Dissertations--Chemical and Materials Engineering, from http://uknowledge.uky.edu/cme_etds/15

[25] A. Abdullah and A. Pak (2008), Correct prediction of the vibration behavior of a high power ultrasonic transducer by FEM simulation, International Journal of Advanced Manufacturing Technology, vol. 39, no. 1–2, pp. 21–28, DOI:10.1007/s00170-007-1191-9.

[26] J. T. Zhao, L. P. Ning, Z. M. Jiang, and Y. L. Li (2021), Design and finite element analysis of longitudinal vibrating stepped ultrasonic horn, Journal of Physics: Conference Series, vol. 2029, no. 1, DOI: 10.1088/1742-6596/2029/1/012056.

[27] A. Abdullah, M. Shahini, and A. Pak (2009), An approach to design a high power piezoelectric ultrasonic transducer, J. Electroceramics, vol. 22, no. 4, pp. 369–382, DOI: 10.1007/s10832-007-9408-8.

[28] D. Hanson, T. P. Waters, D. J. Thompson, R. B. Randall, and R. A. J. Ford (2007), The role of anti-resonance frequencies from operational modal analysis in finite element model updating, Mech. Syst. Signal Process., vol. 21, no. 1, pp. 74–97, DOI: 10.1016/j.ymssp.2006.01.001.

[29] J. Kim and J. Lee (2020), Parametric study of bolt clamping effect on resonance characteristics of langevin transducers with lumped circuit models, Sensors (Switzerland), vol. 20, no. 7, pp. 1–9, DOI: 10.3390/s20071952

[30] I. C. Rosca, M. I. Pop, and N. Cretu (2015), Experimental and numerical study on an ultrasonic horn with shape designed with an optimization algorithm, Appl. Acoust., vol. 95, pp. 60–69. DOI:10.1016/j.apacoust.2015.02.009

[31] H. Razavi, M. Keymanesh, and I. F. Golpayegani (2019), Analysis of free and forced vibrations of ultrasonic vibrating tools, case study: ultrasonic assisted surface rolling process, Int. J. Adv. Manuf. Technol., vol. 103, no. 5–8 , pp. 2725–2737,DOI: 10.1007/s00170-019-03718-x

[32] A. Abdullah, A. Pak, and A. Shahidi (1986), Equivalent Electrical Simulation of High-Power Ultrasonic Piezoelectric Transducers by Using Finite Element Analysis, Ultrasonic.Co.Ir, no. 0, pp. 1–14, from http://ultrasonic.co.ir/files/003.pdf.

[33] M. Y. Baraya and M. Hossam (2020), Design of an electromechanical system for measuring and monitoring micro-ultrasonic amplitude of Langevin transducer, International Journal of Advanced Manufacturing Technology, vol. 107, no. 7–8, pp. 2953–2965, DOI: 10.1016/j.ultras.2019.106002

[34] J. Yu, H. Luo, T. V. Nguyen, L. Huang, B. Liu, and Y. Zhang (2020), Eigenfrequency characterization and tuning of Ti-6Al-4V ultrasonic horn at high temperatures for glass molding, Ultrasonics, vol. 101

[35] Anon, Ieee Standard on Piezoelectricity. USA: New York, N.Y (1978), Institute of Electrical and Electronics Engineers

[36] A. Bybi, H. Drissi, M. Garoum, and A. C. Hladky-Hennion (2019), One-Dimensional Electromechanical Equivalent Circuit for Piezoelectric Array Elements, Adv. Sci. Technol. Innov., pp. 3–9, DOI: 10.1007/978-3-030-05276-8_1

[37] A. A. Vives (2008), Piezoelectric transducers and applications. Springer-Verlag Berlin Heidelberg, DOI: 10.1007/978-3-540-77508-9

[38] F. Sammoura and S. G. Kim (2012), Theoretical modeling and equivalent electric circuit of a bimorph piezoelectric micromachined ultrasonic transducer, IEEE Trans. Ultrason. Ferroelectr. Freq. Control, vol. 59, no. 5, pp. 990–998, DOI: 10.1109/TUFFC.2012.2284.

[39] S. Sherrit, S. P. Leary, B. P. Dolgin, and Y. Bar-Cohen (1999), Comparison of the Mason and KLM equivalent circuits for piezoelectric resonators in the thickness mode, in Proceedings of the IEEE Ultrasonics Symposium, vol. 2, pp. 921–926, DOI: 10.1109/ultsym.1999.849139

[40] Y. Bar-Cohen and K. Zacny (2020), Advances in Terrestrial and Extraterrestrial Drilling.

[41] From: https://philtec.com/wp-content/uploads/2019/06/RC19.pdf, accessed on 2023-02-07

Paper submitted: 21.03.2023.

Paper accepted: 14.08.2023.